MNRAS **000**, 1–7 (2018) Preprint 4 September 2018 Compiled using MNRAS LATEX style file v3.0

Radiation-hydrodynamic simulations of thermally-driven disc winds in X-ray binaries: Increasing luminosity reveals a constant wind efficiency

Nick Higginbottom,[1]⋆ Christian Knigge[1], Knox S. Long[2,3], James H. Matthews[4], Stuart A. Sim[5] and Henrietta A. Hewitt[5].
[1]*School of Physics and Astronomy, University of Southampton, Highfield, Southampton, SO17 1BJ, UK*
[2]*Space Telescope Science Institute, 3700 San Martin Drive, Baltimore, MD, 21218, USA*
[3]*Eureka Scientific Inc., 2542 Delmar Avenue, Suite 100, Oakland, CA, 94602-3017, USA*
[4]*University of Oxford, Astrophysics, Keble Road, Oxford OX1 3RH, UK*
[5]*School of Mathematics and Physics, Queen's University Belfast, University Road, Belfast BT7 1NN, UK*

Accepted XXX. Received YYY; in original form ZZZ

ABSTRACT
The unmistakeable signatures of outflowing gas have been observed in several low-mass X-ray binaries, and evidence from dipping behaviour in a majority of these sources suggests that the outflowing gas is in the form of equatorial disk winds. Whilst the mechanism for the launch and acceleration of these winds is a topic of debate, it is very likely that thermal driving at least contributes to the overall picture. It has been previously demonstrated that thermal winds are able to drive significant outflows (with outflow mass from outer parts of the disk exceeding the accretion rate in the inner disk required to explain the observed source luminosities. Here we use an operator splitting method to carry out radiation-hydrodynamic simulations of a thermally driven disk wind for a range of source luminosities. We find that as the luminosity increases, the wind efficiency (the mass outflow rate scaled to the assumed mass accretion rate) remains constant as a factor of about 2. This is in agreement with both observations and previous theoretical work. We also find that the maximum velocity seen in a simulated absorption line increases with luminosity.

Key words: Accretion discs – hydrodynamics – methods:numerical – stars:winds – X-rays:binaries

1 INTRODUCTION

The signature of outflowing gas has been observed in a vast range of astrophysics objects, from protostellar nebulae through cataclysmic variables and X-ray binaries up to Seyferts and Quasars. Whilst the radio loud jets are the most spectacular form of outflow, it is possible that the slower, yet more massive disk winds may have more impact on the surroundings of the objects and have the ability to change the nature of the accretion flow more substantially. The driving mechanism for these disk winds is a topic of much debate and active research, however there are broadly three contenders.

Firstly, line driving is the process of scattering (mainly UV) radiation from bound-bound lines in ionised material. If the ionisation state of the gas is favourable, then this mechanism can result in a driving force more than 1000 times that expected from Thompson scattering alone (Castor et al. 1975). In X-ray binaries the observed absorption lines suggest that the material thds to be highly ionised (e.g. Kallman et al. 2009; Allen et al. 2018), with ionization parameter $\xi \geq 3$ (Díaz Trigo & Boirin 2016) and hence this mechanism is unlikely to be important. That said, the luminosity of some XRBs is approaching or even exceeding the Eddington limit, and so Thompson scattering alone may be sufficient to affect the flow.

Secondly, thermal driving is the case where gas is heated to a temperature at which the thermal velocity of the gas exceeds the local escape velocity. In this case, mass-loss is inevitable and if the geometry is suitable (for example a geometrically thin accretion disk) then a wind can be produced. This mechanism is particularly attractive in X-ray binaries, where the relatively high temperature of the radiation produced by the inner parts of a black-hole or neutron star accretion disk along with strong X-rays produced by the corona can produce gas temperatures in excess of the escape velocity at reasonable radii. As a rule of thumb, thermal winds might be expected to arise at or just inside the Compton Radius (R_{IC}) - the radius at which gas at the Compton temperature for a given source SED has thermal velocity in excess of the escape

⋆ E-mail: nick_higginbottom@fastmail.fm

velocity (Begelman et al. 1983), defined as

$$R_{IC} = \frac{GM_{BH}\mu m_H}{k_B T_C} \quad (1)$$

where M_{BH} is the mass of the central object, μ is the mean molecular mass which we set to 0.6, and other symbols have the usual meaning.

The third proposed mechanism is that of magneto-centrifugal driving. Observations of the disk-wind in GRO J1655-40 in a peculiar 'hypersoft' state suggested that the wind in that case arose well inside R_{IC}. In such a case the existence of a thermal wind is harder to justify and magneto-centrifugal driving has been suggested as an alternative driving mechanism (Stone & Norman 1992; Miller et al. 2006, 2008; Kallman et al. 2009, but also see Netzer 2006; Uttley & Klein-Wolt 2015; Shidatsu et al. 2016). Since magnetic fields are essential in the evolution of accretion disks, it is not unreasonable to expect such winds to exist. In such a wind, ionized material is loaded onto magnetic field lines leaving the accretion disk, and via a process of angular momentum conservation, the material is accelerated as it moves out along the field lines, like beads on a wire.

Most likely, all three mechanisms are at play perhaps changing their importance depending on the geometry and accretion state of the source in question. Of the three mechanisms, thermal driving is particularly interesting because it is almost certain to operate on some level wherever there is strongly heated gas and a disk of sufficient radial extent that hot gas can escape.

Previous studies have shown that very large mass-loss rates are possible through thermal winds (Higginbottom & Proga 2015) although this is very dependant on the details of the heating/cooling rates (Higginbottom et al. 2017). These in turn depend critically on the source SED and any attenuation effect between the source and the wind launching region. Higginbottom et al. (2018, hereafter H18) presented a radiation-hydrodynamic simulation which took account of this attenuation by coupling the radiative transfer code PYTHON to the hydrodynamics code ZEUS and found that there was still an appreciable outflow, with about 2.5 times as much material outflowing as was required to produced the observed luminosity through accretion. In addition, reasonable agreement was found between Lyman α lines of helium and hydrogen like iron generated from the simulation and those seen in *Chandra* observations of the LMXB GRO J1655-40 in the soft-intermediate state.

That simulation was for a luminosity of 4 percent of the Eddington luminosity (L_{Edd}) for a 7 solar mass central black hole but disk winds have been observed in systems with luminosities up to or even slightly exceeding L_{Edd} (Ponti et al. 2012, herafter P12). Observations suggest that the wind efficiency (mass loss rate divided by mass accretion rate) may increase with luminosity, (P12, although this relationship is driven by observations of a single exceptional source) whilst recent theoretical work suggests that the wind efficiency tends to a constant value (Done et al. 2018, hereafter D18).

Here, we extend the radiation hydrodynamic simulations to higher luminosities in order to investigate the effect on mass loss rate and velocity in the resulting outflows. We use the same technique as H18, and describe the details of the simulations in the next section. We then present our results in Section 3 before making comparisons to observations in Section 4.

2 METHOD

As in H18, we use an operator splitting radiation-hydrodynamic method to treat the propagation of radiation from a central source through the wind. We use the hydrodynamic code ZEUS (Stone & Norman 1992, extended by Proga et al. 2000), coupled to our own ionization and radiative transfer code PYTHON (Long & Knigge 2002, extended by Higginbottom et al. 2013 and Matthews et al. 2015).

Since thermal winds are expected to arise at or just inside R_{IC} which is independent of the source luminosity, we leave the simulation geometry unchanged from H18, and simply increase the luminosity. We use the same logarithmic grid, the parameters of which are given in the upper part of Table 1. The mid-plane of the simulation space is set up with a constant density boundary condition, forming a mass reservoir for any resulting outflow. The value of this constant density is important, since the wind is generated when the ionization parameter is at a critical value $\xi_{cool,max}$ which represents the maximum ionization parameter for gas on the 'cool branch' of the thermal stability curve. Gas with $\xi < \xi_{cool,max}$ has a stable temperature of a few tens of thousands K where line/recombination cooling balances photoionization heating.

As the ionization parameter increases past this value the gas becomes thermally unstable and heats up rapidly. This heating causes expansion and a wind is driven. We refer to the part of the wind where this acceleration occurs as the acceleration zone. In the optically thin limit one can set the mid-plane density so that gas at the mid-plane has exactly the right ionization parameter. This means that the acceleration zone occurs in the cells directly above the mid-plane, avoiding including static material in the simulation, and thus maximizing the resolution in the acceleration zone.

In the simulations presented here attenuation of the radiation is treated fully and it is therefore not possible to compute the ionization parameter for a given cell a-priori since it depends not only on the local density but also on the density of the developing wind along the sightline back to the source. We therefore set the mid-plane density using the optically thin ionisation parameter, finding that a small wedge of static material does form due to optical depth effects. However the extent of this does not significantly affect the resolution in the acceleration zone. The mid-plane density, ρ_0 is given in Table 1 and is proportional to the increasing luminosity, thereby preserving the same ionization parameter (in the optically thin approximation).

All other aspects of the simulation are identical to that described by H18, including a truncation of the mid-plane density boundary condition at $R = 2R_{IC}$.

3 RESULTS

We have computed disk-wind models for central source luminosity $L = 0.1\ L_{Edd} - 1.0\ L_{Edd}$ in steps of $0.1\ L_{Edd}$. In each case, the simulations reach stable states, with static disk-like wedges forming at the base of the simulation as seen in H18. The reason for this structure is attenuation of the radiation through the disk. So, if a cell at a given angle has just the right conditions to launch a wind, the cell behind it will be slightly obscured and so on until at a certain radius the radiation is attenuated to the point at which a wind is launched from the next theta cell 'up'. This gives rise to a thin, slightly convex disk structure.

Because we increase the mid-plane density in proportion to the luminosity in order to try and maintain a fixed ionization parameter

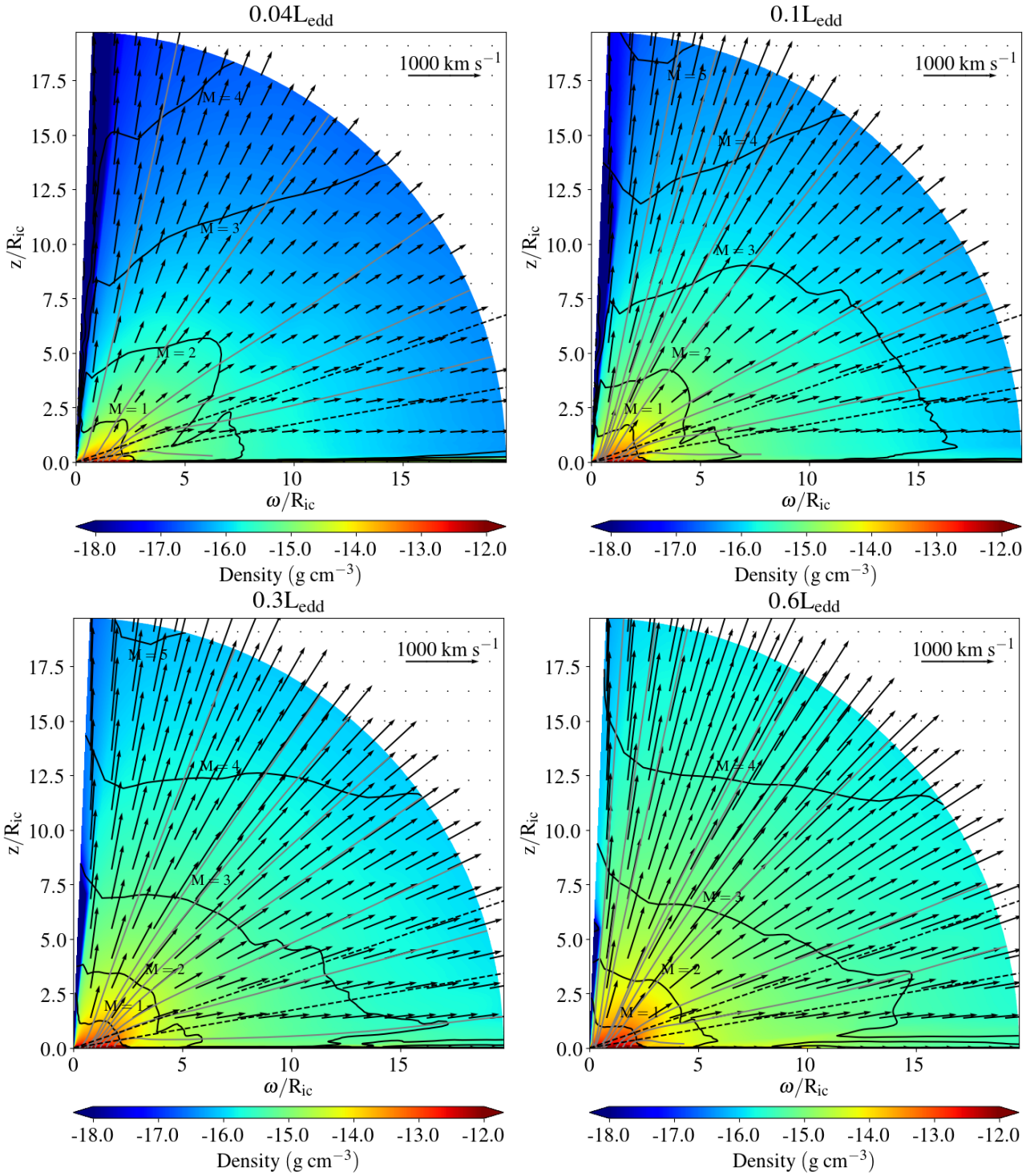

Figure 1. The density and velocity structure of the stable final states for four different luminosities. Grey lines show streamlines, and the black line shows the location of the Mach surfaces. The two dotted lines show the location of the 70° and 80° sightlines.

at the base of the wind, the shape of the disk structure slightly changes as the luminosity increases. In all cases, at the inner radial edge, the disk/wind interface occurs at around 89° from the z-axis (i.e. 1° above the mid-plane). For the original 0.04L$_{\rm Edd}$ simulation, the angle at which the interface occurs decreases to about 88° by the maximum radial extent of the disk, whereas for the L$_{\rm Edd}$ simulation, the interface is about a degree further from the midplane at 87°.

Density contour plots for some of the resulting outflows are shown in Figure 1. We concentrate here, and in the rest of the results/discussion sections, on the calculations using luminosities up to 60 per cent of L_{Edd}. This is because we do not treat continuum driving, a process that would become increasingly important as the luminosity approaches L_{Edd}. It is clear from these images that the velocity of the outflows increases with luminosity, as does the

Luminosity (L_{edd})	0.04	0.1	0.3	0.6
Physical Parameters				
M_{BH} ($M_\odot$)	7	7	7	7
T_x (10^7 K)	5.6	5.6	5.6	5.6
L_x (10^{37} ergs s^{-1})	3.3	8.25	24.75	49.5
M_{acc} (10^{17} ergs s^{-1})	4.42	11.1	33.2	66.3
$\log(\xi_{cold,max})$	1.35	1.35	1.35	1.35
$T_{eq}(\xi_{cold,max})$ (10^3 K)	50.7	50.7	50.7	50.7
ρ_0 (10^{-12} g cm^{-3})	16.0	40	120	240
R_{IC} (10^{11} cm)	4.82	4.82	4.82	4.82
Derived wind properties				
V_r ($\rho > 1 \times 10^{12}$)				
max, blueshifted (km s^{-1})	50	68	256	150
V_r(max, $\theta > 60°$ (km s^{-1})	259	374	533	642
N_H (70°) (10^{22} cm^{-2})	2.0	4.0	8.3	13
N_H (80°) (10^{22} cm^{-2})	4.2	8.4	16	25
$\dot{M}_{wind,outer}$ (10^{18} $g\ s^{-1}$)	1.1	2.7	6.7	12.7
$\dot{M}_{wind,outer}$ ($\dot{M}_{acc}$)	2.5	2.4	2.0	1.9
$0.5\dot{M}V_r^2$ (10^{32} erg s^{-1})	4.2	21.3	109	310

Table 1. Parameters adopted in the simulations, along with key properties of the resulting outflows.

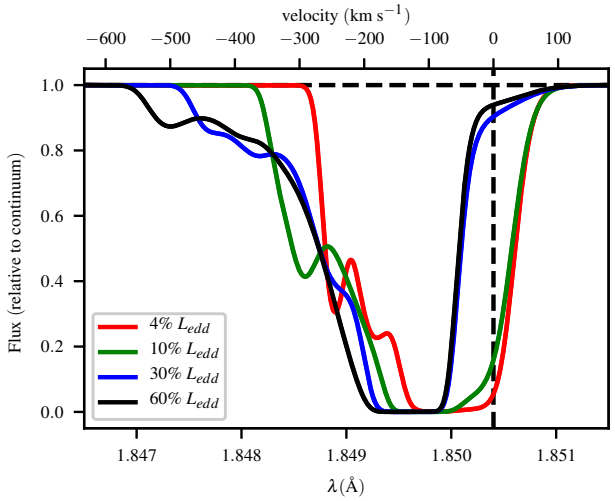

Figure 2. Simulated line profile for the Fe xxv Lyman α transition at 1.85 Å, as viewed from $i = 80°$ for a range of luminosities.

density in the wind. Some useful parameters showing this are given in the lower part of Table 1. As one would expect, the mass-loss rate through the outer boundary, which is essentially a function of these two parameters also increases with luminosity. We will discuss this further in Section 4

We have also computed some simulated absorption line profiles, which give more insight into the velocities in the wind. Firstly, we show the Fe xxv Lyman α transition at 1.85 Å for a sight-line of 80°in Figure 2. This is calculated using the same ray tracing technique as discussed by Higginbottom & Proga (2015). The equivalent width (EW) is very similar for all the lines (because they are all saturated) at about 5-6 eV.

There are two interesting observations to be made from this

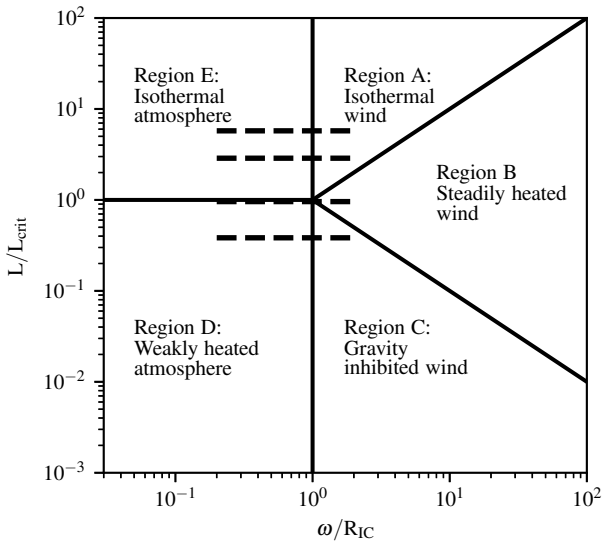

[h]

Figure 3. Regions of different wind solutions after Begelman et al. (1983). The horizontal dashed lines represent the luminosity and disk extent of the simulations in H18 (lowest line) and those presented here

plot. Firstly, the maximum velocity seen in the line increases with luminosity. Secondly, there is a notable difference between the line two lower luminosity profiles and the higher pair. All lines exhibit some absorption at about $+100 kms^{-1}$, due to thermal broadening of absorption from stationary or slow moving material. However for the 4 per cent and 10 percent cases the feature is almost black at $0 kms^{-1}$ indicating the presence of far more slow moving material than in the 30 and 60 per cent cases. An explanation for this can be seen in the expected nature of outflows as one increases luminosity.

A useful way of categorising different classes of thermally driven winds was introduced by (Begelman et al. 1983, hereafter B83), and further developed by (Woods et al. 1996, hereafter W96). The diagram from B83 is reproduced in Figure 3. The vertical axis is the luminosity of the central source in units of the 'critical luminosity' defined as

$$L_{crit} = 0.03 T_{C,8}^{-1/2} L_{Edd} \quad (2)$$

where $T_{C,8}$ is the Compton temperature in units of 10^8 K, whilst the horizontal axis is the radius on the disk where streamline arises normalised to the Compton radius.

The different regions designate different types of outflow or static atmosphere, and are a consequence of how quickly the plasma is heated. The regions in the lower half of the model exhibit slow heating whilst regions in the upper half show rapid heating to the Compton temperature. The regions on the right hand side are where gas at the Compton temperature would be expected to escape, whilst on the left hand side the gas is gravitationally bound and so forms an atmosphere rather than a wind. In region C, the gas is not heated quickly enough to get to the Compton temperature and so the wind is expected to be slow.

B83 found that their model did not yield a clear dividing line between bound and unbound solutions at $\omega = R_{IC}$ and W96 found that a more reasonable location for this cutoff was $\omega = 0.1 R_{IC}$. Our 4 per cent simulation represents about $0.5 L_{crit}$ and is shown on Figure 3 as the lowest horizontal dashed line. The 10 per cent simulation (next horizontal line up) has a luminosity just below

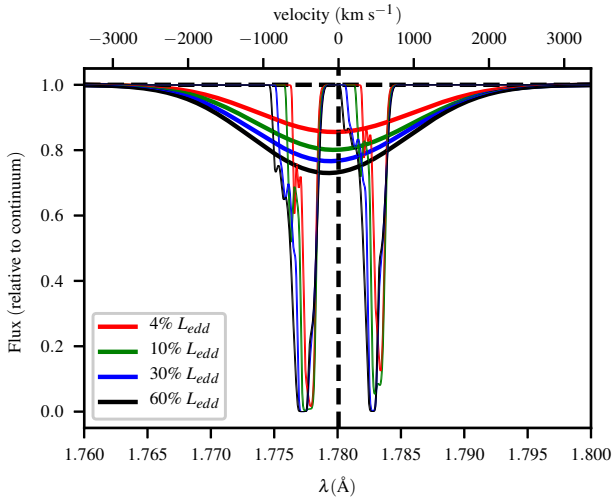

Figure 4. Simulated line profile for the Fe XXVI Lyman α doublet, as viewed from $i = 80°$ for a range of luminosities (thin lines) and also smoothed with a Gaussian to represent the appearance when observed with the*Chandra* HETG with a resolution of 0.012Å (thick lines)

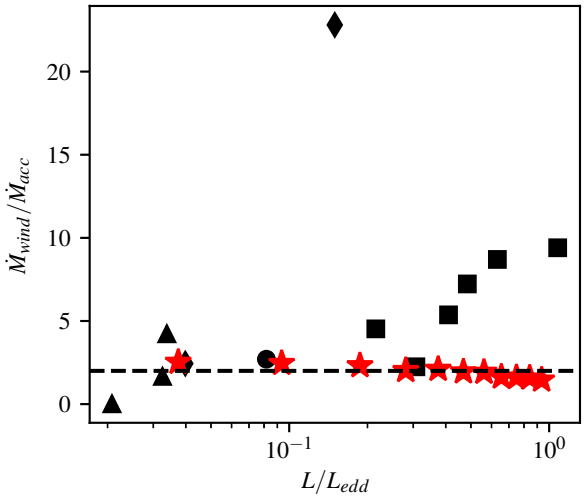

Figure 5. M_{wind}/M_{acc} vs. luminosity based upon figure 5 in Ponti et al. (2012). Black symbols are empirical values obtained from *Chandra* HETG data for several LMXBs. The symbols refer to the specific object each measurement refers to (triangles = H1743-322; circles = 4U 1640-47; squares = GRS 1915+105; diamonds = GRO J1655-40). The red stars represent the results of the simulations presented here, and the dotted line is at M_{wind}/M_{acc}=2.0

L_{crit} and one can therefore tentatively ascribe the difference in the line profile around 0 kms^{-1} to the change from region D/C to region E/B with the gas being more impulsively heated at the higher luminosities and hence accelerating more quickly.

Another line commonly seen in XRB winds is the Lyman α resonance line of Fe XXVI which is actually a doublet with components at 1.778 Å and 1.783 Å. The ray traced absorption profile for this feature is given as the fine lines in Figure 4. Since this feature is less saturated, there is a range of EWs, ranging from -8 eV for the 4 percent L_{Edd} run to -16 eV for the 60 per cent luminosity. The run at the Eddington luminosity has an EW of almost 20eV, but this should be treated with caution because of the lack of continuum driving in our simulation.

The current generation of X-ray spectrometers are unable to split this feature into its components; for example the wavelength resolution of the *Chandra* HETG is 0.012Å compared to the feature spacing of 0.005Å. (Swift XRT = 0.05Å, NuStar = 0.06Å) Therefore the feature is always observed as a single line. The heavy lines in Figure 4 show the line pair smoothed by a Gaussian to reproduce the appearance of this line through the *Chandra* HETG.

I'm unsure about what can we really say here regarding the smoothed line profile. Clearly the line width is huge - I started out thinking I'd write here about how the huge width might mean we kind of see absorption at huge blue shifts (out to the thousands of km/s that is reported in some sources - but in reality presumably observer would fit a Gaussian to this and get a blue shift of a hundred km/s ish w.r.t. to rest wavelength they normally quote of 1.78Å. Not sure that the evidence is here to ruffle feathers

4 DISCUSSION

4.1 Mass-loss rates

The mass-loss rates listed in Table 1 increases as the luminosity of the central source increases however it is interesting to compare these rates with the assumed accretion rate required to generate the luminosity. When we do this we find that the mass-loss through the wind is always roughly double the accretion rate. This 'wind efficiency' relationship is similar to that found in the analysis carried out by Done et al. (2018) who found that for a disk of our size ($R_{out} = 2R_{IC}$) and a Compton temperature very close to ours the wind efficiency peaked at just over two for a luminosity close to our lowest luminosity. They then see the efficiency decrease slowly with increasing luminosity, always remaining above one. Our wind efficiencies are slightly larger than theirs, which is interesting since we neglect any continuum driving effects, which they include via an approximate correction.

The wind efficiency for a range of observed XRB winds is given by Ponti et al. (2012) and it is instructive to compare our results with these observations. Figure 5 shows this comparison, with the black symbols referring to the observations and the red stars showing the results of these simulations.

At first sight, our prediction of a constant wind efficiency does not agree well with the observations, which appear to suggest an increase of wind efficiency with luminosity. However, the trend suggesting an increase in wind efficiency with luminosity is largely driven by observations of just one source - GRS 1915 +105. This is an exceptional source, which has been accreting close to the Eddington limit since its discovery in 1992 (Castro-Tirado et al. 1994; Court et al. 2017) never entering quiescence. It also exhibits unusual SEDs, not corresponding exactly to the normal high/soft, low/hard spectral states Zoghbi et al. (2016). This complex source requires more detailed analysis and modelling which is beyond the scope of this study. Setting aside the observations of this source, thew rest show reasonable consistency with wind efficiency around two over a significant range of luminosities, as seen in the simulations.

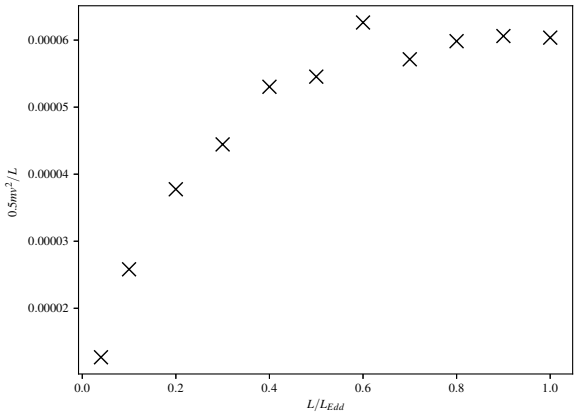

Figure 6. Kinetic energy transported by the wind normalised to the source luminosity as a function of source luminosity.

4.2 Effect of continuum driving

As the luminosity increases, one should include the effects of radiation pressure on the simulation. For such a relatively hard SED, the plasma above the disk will by largely ionized, and so electron pressure would be the only radiation pressure one would expect. The effect can be though of as effectively a reduction in the inner radius at which a wind is launched. Done et al. (2018) give this correction as

$$\overline{R}_{IC} \approx R_{IC}\left(1 - \frac{L}{0.71L_{Edd}}\right). \quad (3)$$

This means that the wind can be launched from all radii at a luminosity of $0.71L_{Edd}$, which means that our mass loss rates will be a lower bound for luminosities approaching or exceeding this value. We might also expect somewhat higher velocities in the outflow, due to the additional force.

I'm thinking that I could include here some numbers extracted from python which give numbers for radiation force- I think it is logged and it would be an interesting first look at what we might expect in the future. Only if its easy though. If not, I think this whole subsection can go

4.3 Kinetic Luminosity

Whilst the mass loss is of interest when considering how the wind could affect the accretion flow through the disk, it is also interesting to consider what (if any) effect the wind could have on the surroundings. The kinetic energy carried by the wind is a good measure of this, and so we calculate this via a simple summation around the outer edge of the domain of massloss rate x radial velocity.

Figure 6 clearly shows a dramatic increase in the 'Kinetic efficiency" of the wind up to about $0.5L_{Edd}$ at which point it seems to reach an asymptotic value of 6×10^{-5} meaning that the wind is capturing about 0.006 per cent of the luminosity of the central source and converting it into kinetic energy. Is this a physically significant number? It is tempting to think one could compute some kind of geometrical interpretation - but the wind covers much more than this tiny percentage of the sky as seen by the central source so there is more to it. In some ways it is more fundamental than the mass loss rate, although probably less important because clearly such small K.Es wont really do much damage outside the system.

5 SUMMARY

Thermal driving is an attractive mechanism to explain the outflows seen in several X-ray binaries seen at high inclinations. We have previously demonstrated that the outflow seen in the soft-intermediate state of GRO J1655-40 could be plausibly modelled by a thermal wind, and here we extend that work to higher luminosities. We find

- As the luminosity increases, so does the mass-loss rate through the wind. However, when one normalizes the mass-loss rate to the assumed accretion rate, the ratio tends to a constant value of around 2. This is in agreement with previous theoretical studies and also observations.
- At the luminosity increases, the maximum blue shifted velocity seen in a simulated absorption line increases. There is also less material at low velocities as the material is more impulsively heated.
- The kinetic energy transported by the wind also increases with luminosity however as with the mass loss rate, the ratio of kinetic energy to luminosity tends to a fixed value of 6×10^{-5}.

6 ACKNOWLEDGEMENTS

Calculations in this work made use of the Iridis4 Supercomputer at the University of Southampton. NH and CK acknowledge support by the Science and Technology Facilities Council grant ST/M001326/1. KSL acknowledges the support of NASA for this work through grant NNG15PP48P to serve as a science adviser to the Astro-H project, JHM is supported by STFC grant ST/N000919/1 and SAS is supported by STFC through grant, ST/P000312/1.

REFERENCES

Allen J. L., Schulz N. S., Homan J., Neilsen J., Nowak M. A., Chakrabarty D., 2018, ApJ, 861, 26
Begelman M. C., McKee C. F., Shields G. A., 1983, ApJ, 271, 70
Castor J. I., Abbott D. C., Klein R. I., 1975, ApJ, 195, 157
Castro-Tirado A. J., Brandt S., Lund N., Lapshov I., Sunyaev R. A., Shlyapnikov A. A., Guziy S., Pavlenko E. P., 1994, ApJS, 92, 469
Court J. M. C., Altamirano D., Pereyra M., Boon C. M., Yamaoka K., Belloni T., Wijnands R., Pahari M., 2017, MNRAS, 468, 4748
Díaz Trigo M., Boirin L., 2016, Astronomische Nachrichten, 337, 368
Done C., Tomaru R., Takahashi T., 2018, MNRAS, 473, 838
Higginbottom N., Proga D., 2015, ApJ, 807, 107
Higginbottom N., Knigge C., Long K. S., Sim S. A., Matthews J. H., 2013, MNRAS, 436, 1390
Higginbottom N., Proga D., Knigge C., Long K. S., 2017, ApJ, 836, 42
Higginbottom N., Knigge C., Long K. S., Matthews J. H., Sim S. A., Hewitt H. A., 2018, MNRAS, 479, 3651
Kallman T. R., Bautista M. A., Goriely S., Mendoza C., Miller J. M., Palmeri P., Quinet P., Raymond J., 2009, ApJ, 701, 865
Long K. S., Knigge C., 2002, ApJ, 579, 725
Matthews J. H., Knigge C., Long K. S., Sim S. A., Higginbottom N., 2015, MNRAS, 450, 3331
Miller J. M., Raymond J., Fabian A., Steeghs D., Homan J., Reynolds C., van der Klis M., Wijnands R., 2006, Nature, 441, 953
Miller J. M., Raymond J., Reynolds C. S., Fabian A. C., Kallman T. R., Homan J., 2008, ApJ, 680, 1359
Netzer H., 2006, ApJ, 652, L117
Ponti G., Fender R. P., Begelman M. C., Dunn R. J. H., Neilsen J., Coriat M., 2012, MNRAS, 422, 11

Proga D., Stone J. M., Kallman T. R., 2000, ApJ, 543, 686
Shidatsu M., Done C., Ueda Y., 2016, ApJ, 823, 159
Stone J. M., Norman M. L., 1992, ApJS, 80, 753
Uttley P., Klein-Wolt M., 2015, MNRAS, 451, 475
Woods D. T., Klein R. I., Castor J. I., McKee C. F., Bell J. B., 1996, ApJ, 461, 767
Zoghbi A., et al., 2016, ApJ, 833, 165
()

This paper has been typeset from a TEX/LATEX file prepared by the author.